Risk Analysis of Wood-frame Residential Buildings Subject to Induced Seismicity Hazard in the Kiskatinaw Region - Northeast British Columbia

Gennaro Esposito, Dalhousie University, Department of Engineering Mathematics, Halifax, NS

May 18, 2023

Abstract

The recent increase of small to moderate induced seismicity in an area between Fort St. John and Dawson Creek, British Columbia, from hydraulic fracturing, has raised concerns on the impact that such events might cause to residential constructions. The induced seismicity is characterized by shallow earthquakes and by short period amplification caused by the nature and geometry of the source and by the subsurface conditions. To estimate the induced seismicity risk for wood-frame residential buildings, we first derive the short-term induced-seismic hazard for the study area. Then, we describe the conditional probability of failure, where failure ranges from minor cosmetic damage to the initiation of collapse. The convolution of the hazard and of the conditional probability of failure allows to estimate the probability of exceedance of each damage level. The model that we used in this study predicts the largest ground motion hazard is in an area aligned along a line joining Dawson Creek and Ft. St. John. This corresponds to the area where most of the hydraulic fracturing activity took place between 2017 and 2018, indicating that most of the wells are potentially seismogenic. The model also predicts probabilities of damage for nay timber frames, any limit state, and any location always two orders of magnitudes smaller than the proposed damage thresholds. Only for the most resilient timber frame model, the model predicts a probability of exceeding the ultimate limit state larger than the target. This is caused by the adopted ground motion model which predicts the highest ground motion intensity at a relatively small period of vibration. Since the most resilient timber frame is a rigid frame having a low period of vibration, the resulting probability of damage is high.

Table of Contents

1. Introduction

The Rocky Mountains, at the boundary between British Columbia and Alberta, are an area of moderate natural tectonic seismicity, but the recent increase of small to moderate seismicity induced by oil and gas extraction in the area (Figure 1) has raised concerns on the impact that such events might cause to residential buildings. The ground motion intensity from induced events can be of comparatively larger amplitude at very short hypocentral distances than that caused by natural earthquakes, as induced events usually occur at shallower depths. In addition, induced earthquakes have large energy at higher frequencies of vibration, becoming potentially damaging for small buildings. At very short hypocentral distances, the ground motion from recent induced events might have exceeded the ground motion from the National Building Code of Canada (hereafter NBC-2015 - NRC, 2015) for tectonic events with 2% exceedance in 50 years (Atkinson et al, 2015).

Hydraulic fracturing (HF, or "injection") is a drilling method used to extract petroleum or natural gas from deep in the Earth. In the injection process, cracks in and below the Earth's surface are opened and widened by injecting water, chemicals, and sand at high pressure. The process results in seismicity at the surface. We conducted a risk analysis of the impact of induced seismicity on typical wood-frame residential structures present in the Kiskatinaw Seismic Monitoring and Mitigation Area (KSMMA – BC OGC, 2018) in British Columbia (BC) (Figure 1), which approximately covers an area of 60 km^2, including the towns of Fort St. John and Dawson Creek. Most of the available literature concerning induced seismicity in the KSMMA focusses on ground motion prediction equations (Atkinson et al., 2016), on the activation rate of seismicity around injection wells (Ghofrani and Atkinson, 2020), on regulation protocols based on either magnitude or human detection (Schultz et al., 2020), and on short term hindcasts of the induced seismic hazard (Ghofrani et al., 2019). The authors are not aware of any past and ongoing research aiming at deriving the ground motion hazard and vulnerability of engineered structures on the surface. The study presented in this paper aims at filling this gap by considering the non-stationary nature of induced seismicity and its impact on buildings. In detail, the objectives of this paper are a) to derive the short-term probabilistic seismic hazard (PSH) related to the amount of hydraulic injection, b) to calculate the seismic vulnerability of residential timber frames conditional on the occurrence of injection, and c) to produce a risk zonation of the study area. The considered failure modes are cosmetic damage (cosmetic limit state – CLS), loss of serviceability (serviceability limit state – SLS), and initiation of structural failure (ultimate limit state, ULS).

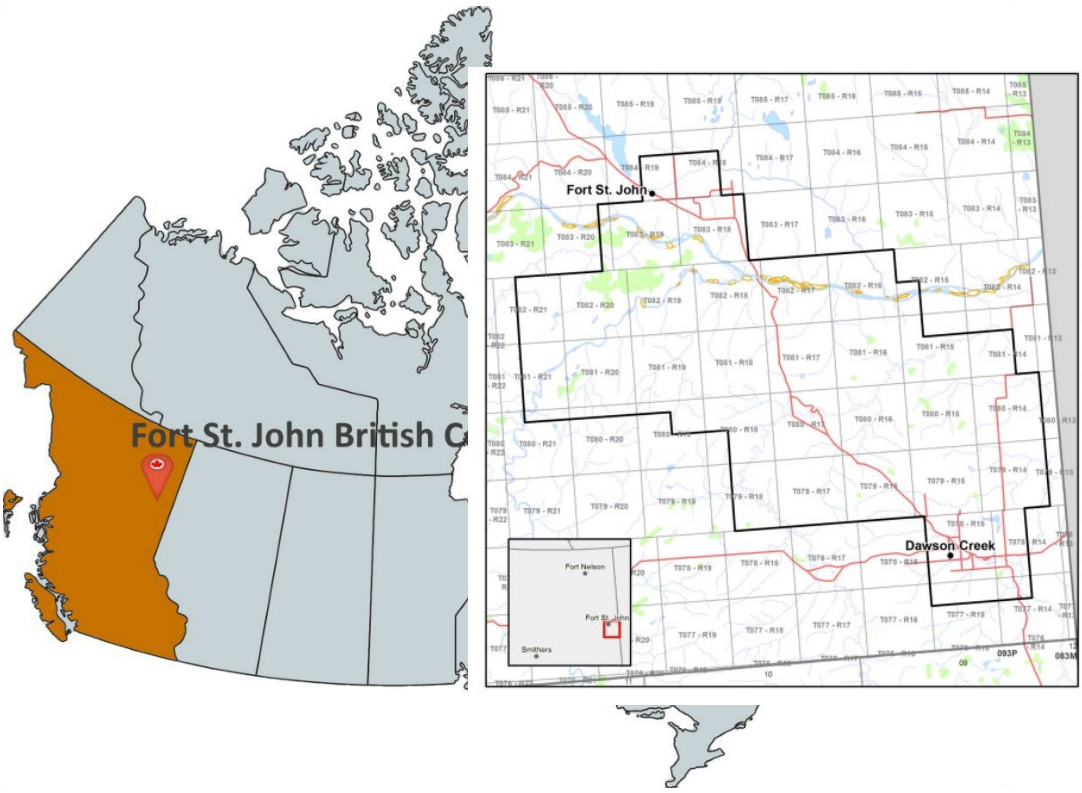

Figure 1 – Location of the Kiskatinaw area

2. Data Selection and Earthquake Catalogue

For the ground motion hazard, we adopt the framework developed by Teng and Baker (2020). Recent research has concluded that the hydraulic-fracturing-induced earthquakes tightly cluster around production wells in space and time (Atkinson et al., 2016; Schultz et al., 2018; Langenbruch et al., 2018; Wang et al., 2018, Hon 2021). Thus, the traditional seismic occurrence model, Poissonian mainshocks with non-stationary aftershock sequences, must be redefined (time limited) in order to compute short-term hazard levels near an active HF operation (Teng and Baker, 2020). Moreover, HF-induced earthquakes have small magnitudes, suggesting that their aftershocks should not have a significant contribution to the hazard level (Teng and Baker, 2020). During the injection time interval, usually a matter of days, we assume that the induced seismicity hazard is Poissonian.

Based on the above observations, a short-term hazard level near a production site is defined as the probability P of exceeding a ground motion intensity $A = a$ over the injection time interval, given the injection activity, i.e. $P[A > a|HF]$. From now on, we drop HF as this seismic hazard model is intended to be always conditional on the occurrence of HF injection. In this study, we use the spectral acceleration A at the fundamental period of the structure, T_o, as the measure of the ground motion intensity for the vulnerability analysis (Goda, 2019). To derive the seismic hazard, we use the 2017-2018 catalogue of earthquakes recorded in the KSMMA and published by NRCan (Visser et al., 2019). The catalogue includes 10,694 earthquakes. From this catalogue, we select the earthquakes associated with production wells based on a spatiotemporal association filter modified from the one proposed by Schultz et al. (2018) as follows:

1. The earthquake occurrence time should be during the period starting at the beginning of the HF operation and ending seven days after well completion (hereafter referred to as the injection time interval).
2. The earthquake hypocenter should be within 6 km from the well surface location (Schultz et al., 2018; Teng and Baker, 2020).

Figure 2 shows the hypocenters of the induced earthquakes and the well locations in the study area selected from the catalogue (Visser et al., 2019). Figure 3 shows the histogram of the earthquake magnitudes.

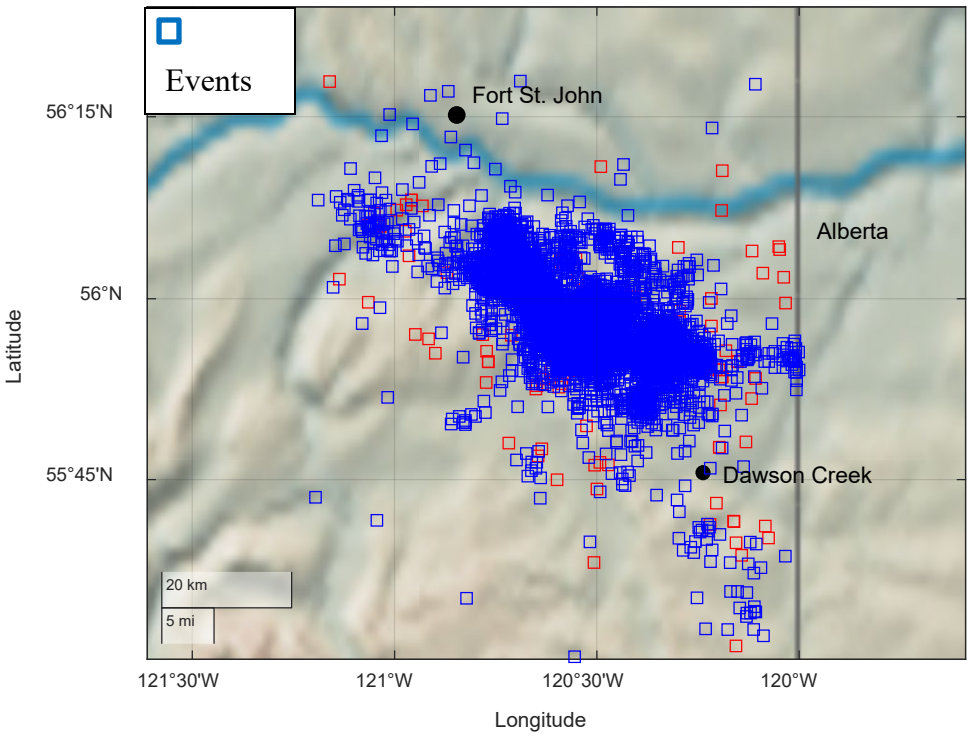

Figure 2 - Earthquake hypocenters and the well locations in the study area.

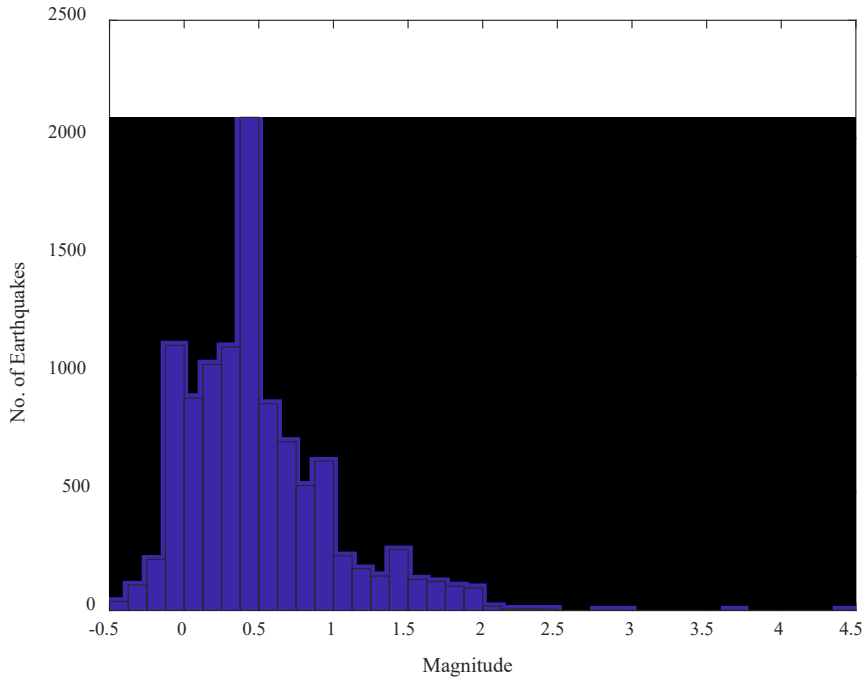

Figure 3 – Histogram of the earthquake magnitudes.

3. Probabilistic Seismic Hazard Analysis Model

The well database of the regulator (BC OGC, 2022) provides coordinates (including depth) and time of each injection. The catalogue of earthquakes recorded in the KSMMA (Visser et al., 2019) provides hypocenter coordinates and the corrected Magnitude $M = m$ of the earthquakes. The problem then becomes to predict the probability that, at a certain site located at the uncertain hypocentral distance $R = r$, the ground motion intensity A exceeds a certain value a . We start with the probability density function of the magnitude M during the injection interval using a Gutenberg-Richter distribution truncated between the magnitude of completeness m_{min} (defined next) and the maximum considered magnitude m_{max} (Cornell and Vanmarcke, 1969)

$$f_M(m) = \frac{\beta_{GR} \cdot exp\{-\beta_{GR}(m - m_{min})\}}{1 - exp\{-\beta_{GR}(m_{max} - m_{min})\}} \quad (1)$$

where β_{GR} is equal to $\ln(10) \cdot b$, and b is the Gutenberg-Richter b-value that characterize the magnitude–frequency relation. The b-value regulates the frequency of smaller earthquakes relative to larger ones: the larger the b-value, the higher the occurrence frequency of smaller events. The magnitude of completeness is the minimum magnitude above which all earthquakes within a certain region are reliably recorded and is defined in the catalogue as $m_{min} = 1.0$ (Visser et al., 2019). Equation 1 is the PDF of the seismic source model (SSM). The ground motion hazard at a certain site is calculated by integrating over all possible magnitudes and distances from the hypocenter as:

$$\mathrm{P}[A > a] = P[S] \cdot \int_{m_{min}}^{m_{max}} \int_0^{R_{max}} P[A > a | m, r] \cdot f_R(R = r) \cdot f_M(m)\, dr\, dm \quad (2)$$

where $P[S]$ is the probability that the well is seismogenic and its derivation is explained later. In Equation 2, $P[A > a|m, r]$ is the ground motion model (GMM) of Atkinson (A2015 - 2015) representing the probability of exceeding a ground motion intensity $A = a$ given the magnitude m earthquake and the hypocentral distance r; $f_R(R = r)$ represents the uncertainty of the distance between source and site, and $f_M(m)$ is calculated with Equation 1. Equation (2) is a modification of the short-term probabilistic hazard model developed by Esposito and Fenton (2022). Since we calculate the hazard using a discrete approximation, Equation (2) is solved numerically as

$$\mathrm{P}[A > a] = P[S] \cdot \sum_{j=1}^{n_m} \sum_{i=1}^{n_r} \mathrm{P}\left[A > a \middle| \Delta m_j, \Delta r_i\right] \cdot \Delta P[\Delta r_i] \cdot \Delta P[\Delta m_j] \quad (3)$$

where $\Delta P[\Delta r_i]$ and $\Delta P\left[\Delta m_j\right]$ are the discretization of the PDFs of R and M respectively (small areas under the PDF's centered on their arguments), n_m and n_r are the number of magnitudes and distances respectively. To obtain the spatial distribution of the hazard in the KSMMA area, we calculate the hazard caused by a hypothetical source located at the center of each cell (defined below). We assume that the seismic sources are disjoint, which means that only one source is active at any certain time. The assumption that the seismic sources are disjoint is reasonable as the probability that two sources cause a damaging earthquake during the same injection time is, for all

practical purposes, equal to zero. In addition, if an earthquake exceeds the ground motion limits given in KSMMA (BC OGC, 2018), operation is immediately shut down. With these assumptions, at any location of the KSMMA region, the total ground motion hazard caused by the sum of any source j present in the KSMMA region (Baker et al., 2021) is

$$P_{tot}[A > a] = \sum_{j=1}^{n_{sources}} P\left[A_j > a | source_j\right] \quad (4)$$

where $n_{sources}$ are all the sources in the study area, $P_{tot}[A > a]$ is the total hazard, and the probability inside the sum is calculated for a single source j using Equation (3). Equation 4 is the seismic hazard during the injection period. The study area is divided into a series of cells, each having area equal to approximately 4,000-by-4,000 m, and Equation 4 is used to estimate the hazard within each cell. Since the ground motion model (GMM) of Atkinson (A2015 - 2015) also provides the distribution of the peak particle velocity (PPV) V, we also derive the ground motion hazard in terms of V as $P[V > v]$. The derivation of the velocity-based ground motion hazard is similar to the one of the acceleration-based ground motion hazard and results in the following expression

$$P_{tot}[V > v] = \sum_{j=1}^{n_{sources}} P\left[V_j > v | source_j\right] \quad (5)$$

4. Parameters Affecting the Hazard Model

Maximum Magnitude

The parameter m_{max} is critical for the ground motion hazard. A recent study in the KSMMA (Pena Castro et al., 2020, Li et al., 2022) revealed that m_{max} equal to 5 is to be considered as the most likely maximum magnitude in the Western Canadian Sedimentary Basin for HF. To check this conclusion, we consider the maxima, M_{max}, to be exponentially distributed as

$$\lambda[M_{max} > m_{max}] = k_1 \cdot \exp(-k_2 \cdot m_{max}) \quad (6)$$

where λ is the rate, and k_1 and k_2 are regression constants. M_{max} distribution is shown in Figure 4 with the observed annual values of m_{max}. Considering the induced earthquakes as Poissonian, the return period is $RP = 1/\lambda$. Considering that the design life of new buildings is 50 years, we are interested in earthquakes having return periods of 50 years, or λ = 1/50 = 0.02/annum. Using λ = 0.02 on the left-hand-side of Equation 6 gives m_{max} equal to 6. Existing timber frames in the study area might be close to, or have exceeded their design life, and as a consequence a lower m_{max} should be selected since their remaining lifetime may be significantly less than 50 years. In this study, we use m_{max} equal to 5 in alignment with (Pena Castro et al., 2020, Li et al., 2022). In addition we investigate the seismic vulnerability of the timber frames using our estimated m_{max} equal to 6, which should be considered as a conservative parameter.

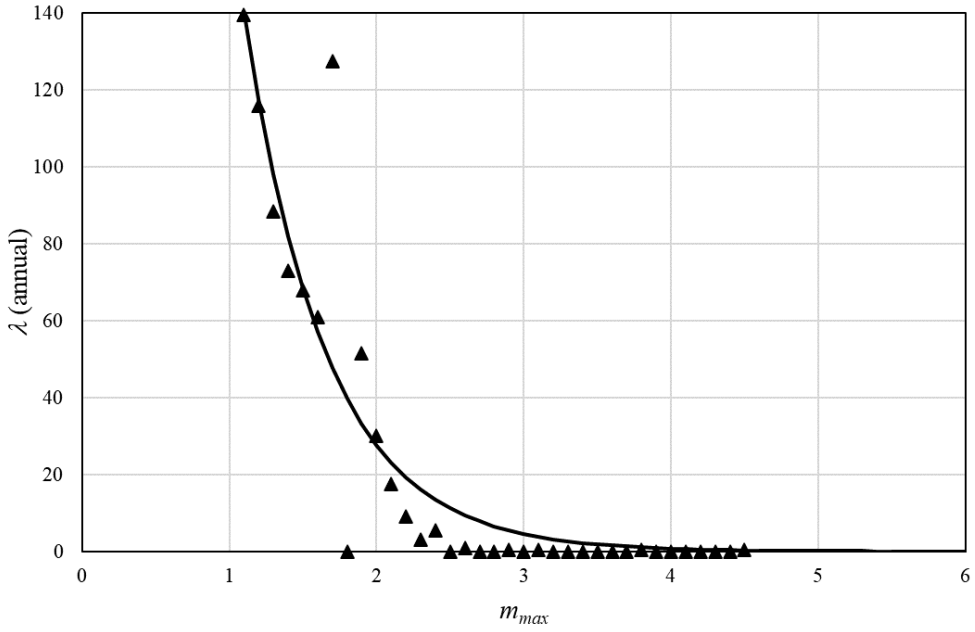

Figure 4 – Distribution of M_{max} and observed annual m_{max}

Probability of Being Seismogenic

The hazard model, Equation5, represents the sum of the hazard from all the possible sources $n_{sources}$ in the study area and implies that all the $n_{sources}$ are equally likely to cause an earthquake. In reality, only a fraction of the wells in the regulator database (BC OGC, 2022) have triggered earthquakes, most likely for geological reasons which are beyond the scope of this study. To estimate if a source (a well) is seismogenic or not, we introduce the binary categorical variable $I(\boldsymbol{x_k})$, set to 1 if the sampled location with coordinate $\boldsymbol{x_k}$ is seismogenic, and to 0 if not. To estimate the value of $I(\boldsymbol{x})$ at unsampled locations, we apply indicator kriging (Deutsch and Journel, 1997) that provides a least-squares estimate of the categoric variable $I(\boldsymbol{x})$ at unsampled locations. The estimate is written as (Deutsch and Journel, 1997):

(7) $$\hat{I}(\boldsymbol{x}) = \sum_{i=1}^{n} \beta_i I(\boldsymbol{x_i})$$

where β_k are the coefficients of the linear combination. Equation (7) is an estimate of $P[I(\boldsymbol{x}) = 1]$. The coefficients β_k have to be selected in order to have an unbiased estimator which also has the smallest possible estimation variance. Assuming stationarity, one has:

(8) $$E[I(\boldsymbol{x})] = m$$

where m is the mean of the random field and $E[\,]$ is the expected value operator. This means for the linear estimator

(9) $$E[\hat{I}(\boldsymbol{x})] = \sum_{i=1}^{n} \beta_i E[I(\boldsymbol{x_i})] = m$$

Therefore, the weights have to fulfil

(10) $$\sum_{i=1}^{n} \beta_i = 1$$

The estimation variance can be calculated with the help of the semi-variance function $\gamma(\boldsymbol{h})$, where $\boldsymbol{h}$ is the separation distance vector between two sampled wells having coordinates $\boldsymbol{x}$ and $\boldsymbol{x} + \boldsymbol{h}$. as:

(11) $$\sigma^2(\boldsymbol{x}) = var\left[I(\boldsymbol{x}) - \hat{I}(\boldsymbol{x})\right] = -\sum_{j=1}^{n}\sum_{i=1}^{n} \beta_j \beta_i \gamma(\boldsymbol{x_i} - \boldsymbol{x_j}) - 2\sum_{i=1}^{n} \beta_i \gamma(\boldsymbol{x_i} - \boldsymbol{x})$$

The best linear unbiased estimator (BLUE – Fenton and Griffiths, 2008) is the one which minimizes the estimation variance with respect to the unbiasedness condition. This constrained optimization problem can be solved with the help of a Lagrange multiplier μ. The function

(12) $$\sigma^2(\boldsymbol{x}) - 2\mu\left(\sum_{i=1}^{n} \beta_i - 1\right)$$

is to be minimized. Using the partial derivatives with respect to the unknown parameters β_i and μ one has to solve the linear equation system:

$$\sum_{j=1}^{n} \beta_j \gamma(\boldsymbol{x_i} - \boldsymbol{x_j}) + \mu = \gamma(\boldsymbol{x_i} - \boldsymbol{x}) \qquad i = 1, \dots, n$$

(13)

$$\sum_{i=1}^{n} \beta_i = 1$$

For the study area, we use the following exponential theoretical model

(14) $$\gamma(\boldsymbol{h}) = C(0)(1 - e^{-\frac{|h|}{d}})$$

where $C(0)$ is the covariance calculated at the separation distance equal to zero and is a nonnegative value and d is the correlation length. The resulting estimate of $\hat{P}[I(\boldsymbol{x}) = 1]$ is shown in Figure 5.

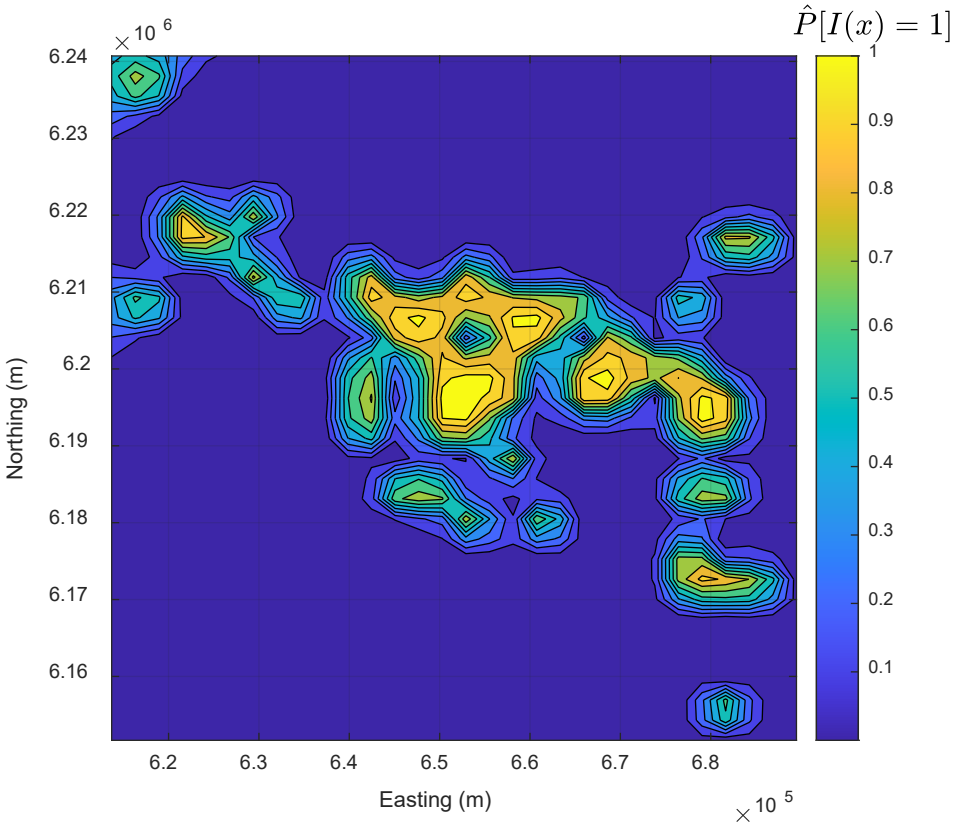

Figure 5 – Estimate of $\hat{P}[I(\boldsymbol{x}) = 1]$

Determination of β_{GR}

The parameter β_{GR} was estimated from b using the maximum likelihood method given by Aki (1965). We derive b with the expressions below:

(15) $$b = \frac{1}{\log_{10} e\,[\mu_M - m_{min}]}$$

where μ_M is the mean magnitude of the catalogue. From Equation (15), β_{GR} can be derived using the relationship $\beta_{GR} = \ln(10) \cdot b$. From the catalogue, the estimated b is 1.1 so that β_{GR} is equal to 2.53.

5. Seismic Capacity of Residential Timber Frames

5.1 Acceleration-Based Seismic Capacity

Let $A = a$ be the ground motion acceleration hazard experienced at a site, and F_A the probability of failure in terms of the ground motion acceleration. Assuming that F_A is lognormally distributed (Baker and al., 2021) with parameters $\mu_{\ln C_A}$ and $\sigma_{\ln C_A}$, then the probability of failure conditional to the occurrence of $A = a$ is

$$P[F_A|A = a] = \Phi\left(\frac{\ln\left(\frac{a}{\mu_{\ln F_A}}\right)}{\sigma_{\ln F_A}}\right) \tag{16}$$

The conditional probability of failure used in this study are based on the UBC-SAWS model of typical wood-frame houses in British Columbia (White and Ventura, 2006), which in turn is a refinement of the SAWS model (Folz and Filiatrault, 2004). We consider four two-storey timber frames houses models (house hereafter) having different shear-walls:

- House 1 has shear walls made of stucco and engineered oriented strand board (OSB) or gypsum wallboard (GWB).
- House 2 has shear walls made of engineered OSB/GWB,
- House 3 has shear walls made of non-engineered OSB/GWB, and
- House 4 has sheal walls consisting of horizontal boards or GWB.

The term "engineered" indicates the presence of hold-downs and blocking of the wall panel to increase its seismic resistance and to meet the seismic code requirements. We consider four limit states corresponding to four levels of damage, slight (F_{A1}), moderate (F_{A2}), extensive (F_{A3}), and collapse (F_{A4}). Each F_A corresponds to increasing levels of inter-storey drift ratio (Goda, 2019). With this notation, Equation (16) becomes

$$P[F_{Ai}|A = a] = \Phi\left(\frac{\ln\left(\frac{a}{\mu_{\ln F_{Ai}}}\right)}{\sigma_{\ln F_{Ai}}}\right) \tag{17}$$

where F_{Ai} is the conditional damage level i with $i = 1, \ldots, 4$. F_{A1} represents the initiation of wall and ceilings cracks. F_{A2} corresponds to the presence of many cracks on the walls and ceilings, this could be interpreted as the cosmetic damage limit state (CLS). F_{A3} is the serviceability limit state (SLS), for instance the presence of jammed doors or windows. Finally, F_{A4} represents the initiation of collapse of the structure (ultimate limit state – ULS). The maximum inter-storey drift ratios for each house and damage state are summarized in Table 1.

Table 1 - Maximum inter-storey drift ratios for each house model and damage state

	F_{A1}	F_{A2}	F_{A3}	F_{A4}
House 1	0.005	0.01	0.035	0.07
House 2	0.005	0.01	0.03	0.06
House 3	0.005	0.01	0.03	0.06
House 4	0.005	0.01	0.025	0.05

The damage thresholds for F_{A4} (ULS) are chosen based on White and Ventura (2006), Christovasilis et al. (2009), and Pan et al. (2018), whereas those for F_{A3} (SLS) are set to 50% of F_{A4}. We consider only the house vibration direction along the longest frame side, where the fundamental vibration periods are assumed to be 0.25, 0.3, 0.35, and 0.4 s, for house models 1, 2, 3, and 4 respectively.

Goda (2019) developed a national earthquake risk model for wood-frame houses in Canada and calibrated the conditional probabilities of failure for 1620 postal code locations. We performed few pushover analyses of the four houses (not shown in this paper) under different tectonic earthquake conditions and plotted the results on the conditional probabilities of failure derived by Goda (2019). Our structural analysis results substantially matched the conditional probability parameters calculated by Goda (2019) for the postal codes close to the study area. The calculated parameters $\mu_{F_{Ai}}$ and $\sigma_{F_{Ai}}$ used in this study are shown in Table 2. The conditional probabilities of failure for the four houses are shown in Figures 6. In terms of seismic resistance, inspecting the fragility curves it appears that House 1 has the highest seismic capacity. Houses 2 and 3 have similar seismic resistance, whereas House 4 has the lowest seismic capacity. House 1 may be considered as a modern seismic resistant timber frame, whereas Houses 2 and 3 may be considered as typical seismically engineered houses in western Canada. Finally, House 4 represents a not seismically engineered timber frame.

Table 2 - Parameters $\mu_{F_{Ai}}$ and $\sigma_{F_{Ai}}$ of the conditional probability of failure

		F_{A1}	F_{A2}	F_{A3}	F_{A4}
house 1	μ_{F_A}	-0.224	0.354	1.131	1.267
	σ_{F_A}	0.228	0.237	0.298	0.297
house 2	μ_{F_A}	-0.393	0.182	0.822	1.021
	σ_{F_A}	0.258	0.276	0.324	0.327
house 3	μ_{F_A}	-0.553	0.117	0.777	0.946
	σ_{F_A}	0.285	0.288	0.331	0.332
house 4	μ_{F_A}	-0.744	-0.163	0.454	0.655
	σ_{F_A}	0.315	0.316	0.339	0.361

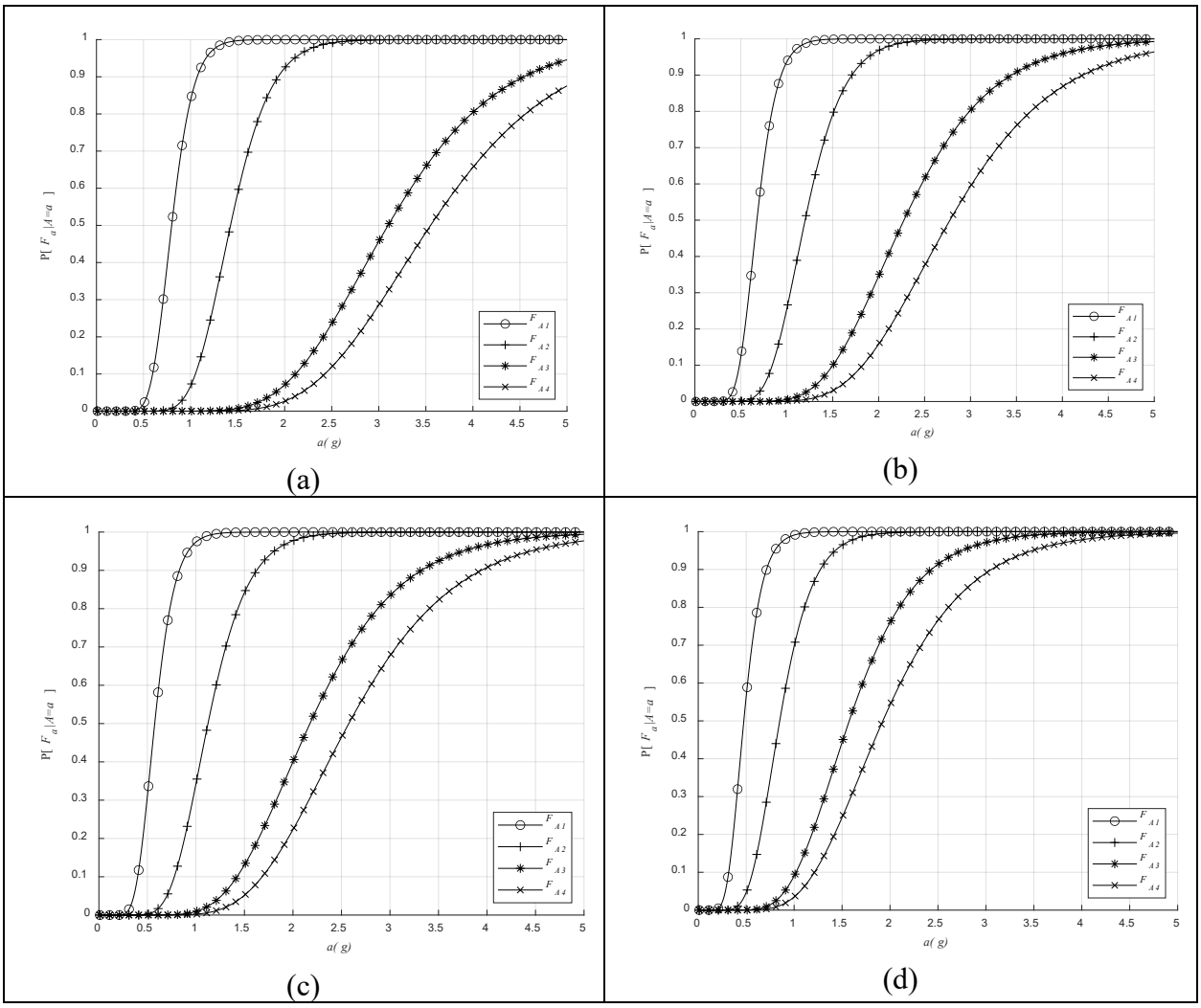

Figure 6 – Conditional probability of failure of House 1 (a), House 2 (b), House 3 (c), and House (4).

5.2 Velocity-Based Seismic capacity for CLS

The convolution of the acceleration-based conditional probability of failure F_{A2} presented previously (Equation 17) with the ground motion hazard (Equation (5)) allows to directly determine the unconditional probability of cosmetic damage $P[F_{A2}]$. Traditionally, probability of cosmetic damage is assessed considering the peak particle velocity (PPV), $V = v$, rather than acceleration. The most advanced vibration-induced damage standards are based on PPV and are produced in several European countries, for instance the German DIN 4150–3 (2016), the Dutch SBR-A guideline (SBRCURNET, 2017), and the British BS 7385-2 (BSI,1993). The drawback of the European standards is that they mostly focus on masonry buildings and walls, therefore their application to timber frames is not straightforward. To assess the probability of cosmetic damage, we use herein USBM RI 8507 (USBM, 1983). Although this standard applies to timber frames, it

is based on older construction methodologies that are not directly applicable to more modern residential construction practice. Figure 7 shows the USBM RI 8507 (USBM, 1983) limits as function of the fundamental vibration frequency of the timber frame, $f = 1/T$. Figure 7 also shows the fundamental frequencies for the four houses considered in this study. The velocity limits, v, are summarized in Table 3.

The correct interpretation of USBM RI 8507 (USBM, 1983) is critical to understand the probability of cosmetic damage when the limits are exceeded. The standard was developed for blast-induced vibrations, usually having short duration. The black lines in Figure 7 are the limits corresponding to 5% probability damage for a given single blasting-caused vibration, lasting less than a few seconds. Thus, if $V = v$ is at or below the black line, $P[F_{V2}|V = v]$ is equal to or less than 5%. The limits in Figure 7 are applicable if the house is essentially intact, lays on firm foundations, is a timber frame, two stories or less in height, and has typical "dimensions". Note that what is "typical" in USBM RI 8507 (USBM, 1983) may not be typical in more modern residential timber frames. With these limitations, in this study we assume that the black lines in Figure 7 represent a probability of cosmetic damage equal to 5% also for timber frames built with more modern construction methodologies. Using the data set collected to develop USBM RI 8507 (USBM, 1983), we matched a lognormal distribution at each frequency corresponding to the four houses used in this study. The derived distribution parameters $\mu_{\ln F_{V2}}$ and $\sigma_{\ln F_{V2}}$ are summarized in Table 4. The distributions are in Figure 9.

Table 3 – Vibration damage limits for the four house-models considered in this study

Type	Plaster (mm/s)	Drywall (mm/s)
house 1	13	19
house 2	13	15
house 3	13	13
house 4	11	11

Table 4 – Logarithmic mean and standard deviation for the velocity-based conditional probability of failure for the four house-models considered in this study

Type	Plaster	Drywall
house 1	$\sigma_{\ln F_{V2}} = 0.55$ $\mu_{\ln F_{V2}} = 1.24$	$\sigma_{\ln F_{V2}} = 0.5$ $\mu_{\ln F_{V2}} = 1.34$
house 2	$\sigma_{\ln F_{V2}} = 0.55$ $\mu_{\ln F_{V2}} = 1.24$	$\sigma_{\ln F_{V2}} = 0.53$ $\mu_{\ln F_{V2}} = 1.28$
house 3	$\sigma_{\ln F_{V2}} = 0.55$ $\mu_{\ln F_{V2}} = 1.24$	$\sigma_{\ln F_{V2}} = 0.55$ $\mu_{\ln F_{V2}} = 1.24$
house 4	$\sigma_{\ln F_{V2}} = 0.5$ $\mu_{\ln F_{V2}} = 1.15$	$\sigma_{\ln F_{V2}} = 0.5$ $\mu_{\ln F_{V2}} = 1.15$

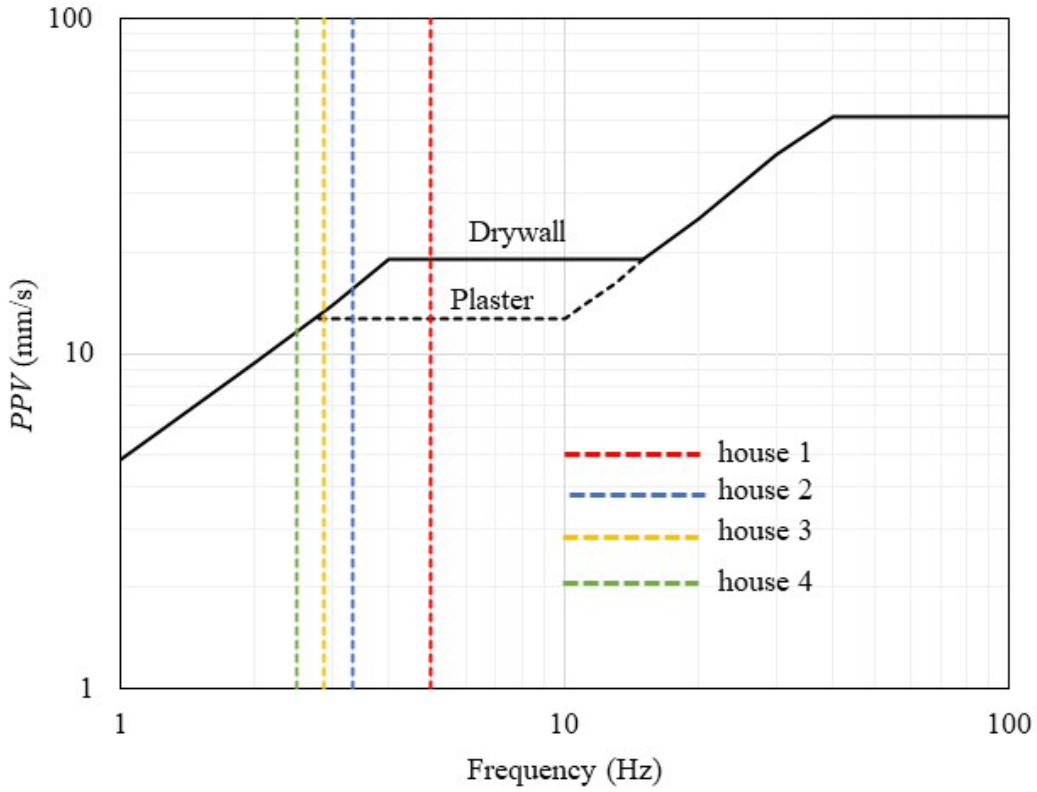

Figure 7 – Vibration damage thresholds (USBM, 1983).

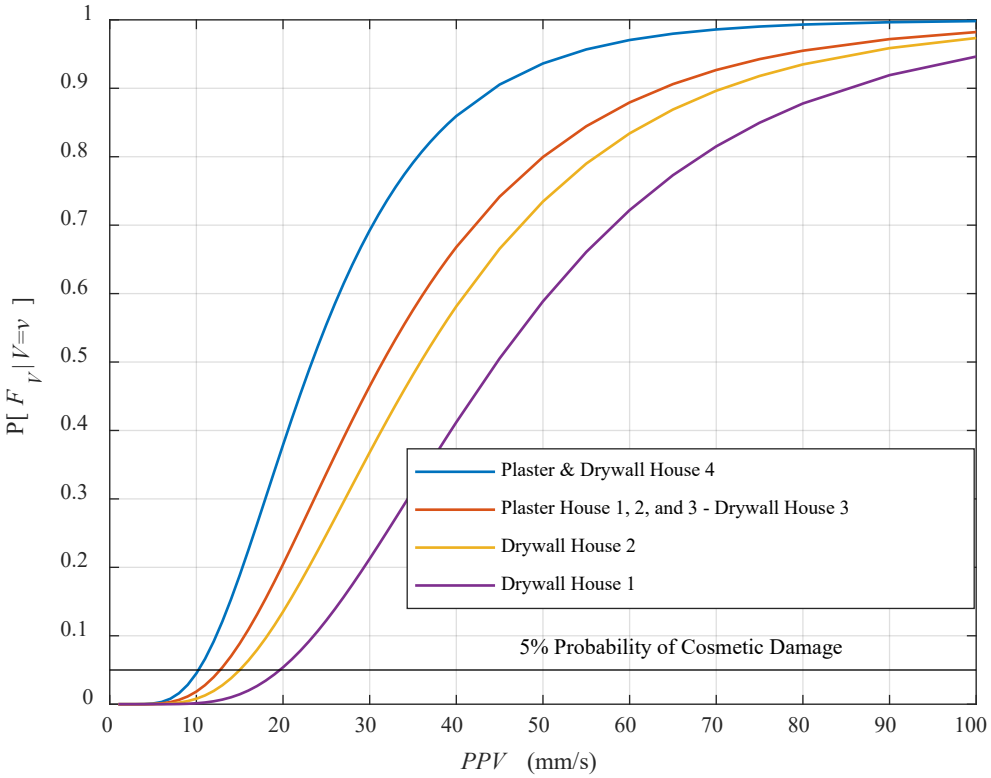

Figure 8 – Velocity-based conditional probability of failure for CLS

6. Unconditional Probability of Damage

The acceleration-based unconditional damage rate for limit state i, F_{Ai}, during the injection interval (7 days) is

$$P[F_{Ai}] = \int_0^\infty P[F_{Ai}|A = a] \cdot f_A(a)\, da \tag{18}$$

Where $f_A(a)$ is calculated from Equation 4 as

$$f_A(a) = \frac{d\,(1-P_{tot}[A>a])}{da} \tag{19}$$

We solve Equation (19) numerically as

$$P[F_{Ai}] = \sum_{k=1}^{a_{max}} P[F_{Ai}|A = a_k] \cdot P[A = a_k] \tag{20}$$

where a_{max} is the maximum calculated ground motion acceleration hazard. Similarly, the velocity-based unconditional probability damage for CLS is

$$P[F_{V2}] = \sum_{k=1}^{v_{max}} P[F_{V2}|V = V_k] \cdot P[V = v_k] \tag{21}$$

where $P[V = v_k]$ is obtained from a discretization of $f_V(v)$ (Equation (5)) as

$$f_V(v) = \frac{d\,(1-P_{tot}[V>v])}{dv} \tag{22}$$

Since building codes are often expressed in terms of annual probabilities of failure, we are interested in the probabilities $P[F_{Ai}]$ and $P[F_{V2}]$ in one year. Assuming that the occurrence of the limit state follows a Poisson process in time, and that T_1 is the first (or next) occurrence of a limit state, then

$$P[F_{Ai}] = P[T_1 \leq t] = 1 - \exp\{-\lambda t\} \tag{23}$$

where t is the time interval and λ is the mean rate of the limit state occurrence. Since the hazard is calculated for an injection time interval, one injection time interval (7 days) is assumed to correspond to t = 1. Thus, with t=1, the limit state mean rate of occurrence λ is

$$\lambda[F_{Ai}] = -\ln\,(1 - P[F_{Ai}]) \tag{24}$$

Considering that in one year there are approximately 52 weeks, we can write the annual probability of observing at least one limit state as

$$P[F_{Ai}]_1 = P[T_1 \leq 52] = F_{T_1}(t) = 1 - \exp\{-\lambda[F_{Ai}] \cdot 52\} \tag{25}$$

7. Limit States Targets

To assess the damage potential for the residential timber frames in the study area, we must consider the available regulation and guidelines for CLS, SLS, and ULS. For completeness, in this study the damage state C_{A1} is calculated but not assessed against any target as the authors did not find any useful reference in literature.

CLS

It is recognized that there is no precise level at which cosmetic damage begins to occur. The damage level depends on the type, condition, and age of the structure, the soil conditions on which the structure is built, and the frequency of the vibration. For velocity-based assessment, the statistical nature of the USBM standard (1983) means that not all vibrations which are deemed "allowable" (e.g. below the threshold lines in Figure 7) in a given setting and standard will be non-damaging to all houses in all circumstances. Similarly, not all vibrations deemed "non-allowable" (those above the threshold lines of Figure 7) will always cause visible damage. Finally, USBM standard (1983) is intended for continuous short-lasting blast-induced vibrations. In terms of occurrence and duration, the induced earthquakes are comparable to the blast-induced vibrations. In absence of provincial guidelines, for vibration-based CLS assessment, we propose using $P[F_{V2}]_1 = 5\%$ per year, or one in twenty, meaning that if PPV is at or below this limit, 95% of intact houses on firm foundations, two stories or less in height, having the dimensions of typical residences, will not be damaged by that PPV. For the acceleration-based CLS assessment, we use a similar threshold of 5% per annum. Using Equation 25, this corresponds to $P[F_{V2}]_1 = P[F_{A2}]_1 = 0.001$ or one in thousand for the injection interval.

SLS

The National Building Code of Canada commentary (NBC – NRC, 2020) provides limiting values for structural deformation (displacements and rotations), however it does not provide a target probability of occurrence or exceedance during the design life. The target probability of SLS damage occurrence is not well documented in literature as most of the engineering interest is on ULS, which is relevant for life safety. Usually, it is accepted that the probability of failure for SLS can be larger than the probability of failure for ULS. Acceptable annual probability of failures for ULS seem to be around 1 in thousand or less (see later), thus acceptable probability of failures for SLS should be larger, say in the range of 1 in hundreds or less.

Eurocode 0 (CEN, 2003) sets the target reliability for irreversible SLS in Annex C as β_1=2.3 for a 1-year reference period for structures with medium consequences of failure (e.g. residential and office buildings, public buildings). It is possible to transform the annual reliability index in an annual probability of failure as

(24) $$P[F_{A3}]_1 = 1 - \Phi(\beta_1) = 1 - \Phi(2.3) = 0.01$$

The Joint Committee on Structural Safety (JCSS, 2000) proposes an annual (irreversible) probability of failure for the SLS and normal importance structures such as residential buildings of 0.05. For this study, we propose to use $P[F_{A3}]_1 = 0.01$ as threshold meaning that the probability of irreversible SLS damage should be equal or less than 1 in 100 per annum. Assuming independence of the induced-seismic earthquakes, this corresponds to $P[F_{A3}]_1 = 0.0002$, or 1 in five thousand, for the injection period.

The suitability of this target for SLS is a difficult topic that would require a dedicated research project and goes beyond the scope of this study. The authors of this report recommend to investigate acceptable SLS limits in further research efforts as, in the author opinion, this limit state and CLS are relevant for the study area.

ULS

The NBC (NRC, 2020) is mute on the target probability of failure for ULS (life safety) for a building designed to resist an earthquake according to the code provisions. NBC (NRC,2020) provisions are given to design structures able to resist ground motion intensity having an annual probability of occurrence of 0.000404 corresponding to a return period of 2,475 years. The ULS probability of failure of a building designed according to the NBC (NRC, 2020) provisions is therefore unknown.

To assess the calculated $P[F_{A4}]_1$ in the study area, we suggest adopting the target probability of failure given in the American code ASCE-7 (ASCE, 2022). For new residential building similar to those considered in this study, ASCE-7 (ASCE, 2022) prescribes that the probability of failure conditional to the occurrence of the design earthquake in 50 years, $P[F_{A4}]_{50}$, must be smaller than 10%. Assuming that each year is independent and using Equation 24, this corresponds to an annual $P[F_{A4}]_1$ of 0.002, or 1 in five hundred, where the design earthquake in this case is an induced seismic earthquake. This value is very close to what the authors of this paper believe is the current performance of residential structures built according to the Canadian code. Assuming independence of the induced-seismic earthquakes and using Equation 23, this corresponds to the probability of failure for the injection period $[F_{A4}]_1 = 0.00004$, or 1 in twenty-five thousand.

Summary of the proposed damage thresholds

The proposed damage thresholds are summarized in Table 4.

Table 4 – Summary of the damage thresholds

Limit State	$P[F_{Ai}]$ – Injection Period	$P[F_{Ai}]_1$ – 1 year
CLS*	1.00E-03	5.00E-02
SLS	2.00E-04	1.00E-02
ULS	4.00E-05	2.00E-03

*For both acceleration- and velocity-based conditional probability of failure

8. Calculated Ground Motion Hazard

The ground motion hazard results are presented in maps for the peak velocity $V = v$ and the spectral acceleration $A = a$ at the periods $T = 0.25$ (the fundamental vibration period of the most resilient house, House 1) and $T = 0.4\ s$ (the fundamental vibration period of the most vulnerable house, House 4) for one year period. For each T we plot $P[V > v]$ at v equal to 11, 13, 15, and 19 mm/s, and $P[A > a]$ at a equal to 0.05 g, 0.1 g, 0.2 g, and 0.5 g. The ground motion hazard is shown in Figures 9 to 11. Comparing these figures with Figure 2 showing the location of the wells and the epicenters of the events, the ground motion hazard is the largest where the largest number of earthquakes was recorded. The density of the wells is not the only factor affecting the hazard. Certain areas characterized by intense fracking, experience a relatively low hazard, possibly due to favorable or unfavorable effect of geological features. Inspection of Figures 9 and 11 also indicates that the spectral acceleration hazard decreases as the vibration period T increases. This is due to the GMM A2015 (Atkinson, 2015) that predicts the largest hazard at vibration periods smaller than T = 0.2 s. The GMM A2015 (Atkinson, 2015) was derived from available seismic records and represents the distinctive high-frequency spectral features of recorded induced earthquakes. This model is widely accepted among the researchers working in this area. It is important to note that the GMM model is limited to records acquired at relatively long distance, for shallow earthquakes, from the source. Therefore, shorter-distance lower-frequency features of induced earthquakes or pulse-effects caused by directional effects are not captured by the GMM A2015 (Atkinson, 2015) model. The impact of GMM A2015 (Atkinson, 2015) on the timber frames probability damage is discussed in the next section.

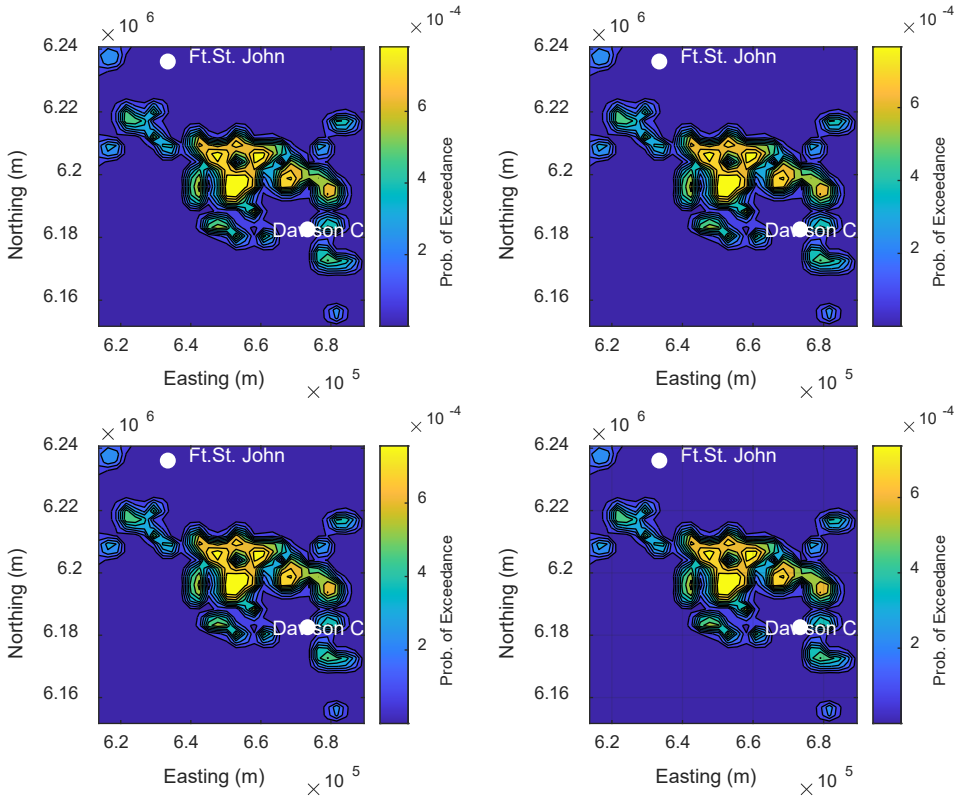

Figure 9 – Hazard $P[V > v]$, with $v = 11\ mm/s$ (top left), $v = 13\ mm/s$ (top right), $v = 15\ mm/s$ (bottom left), and $v = 19\ mm/s$ (bottom right).

bottom left), and $v = 19\ mm/s$ (bottom right).

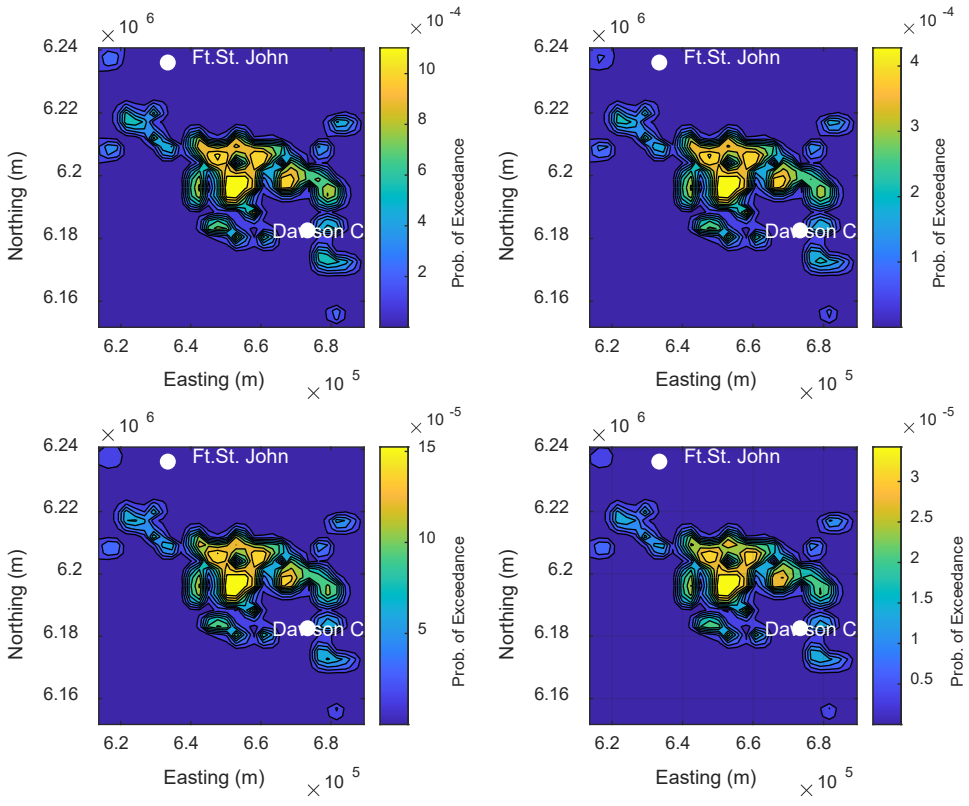

Figure 10 – T = 0.25 s, hazard $P[A > a]$, with $a = 0.05\ g$ (top left), $a = 0.1\ g$ (top right), $a = 0.2\ g$ (bottom left), and $a = 0.5\ g$ (bottom right).

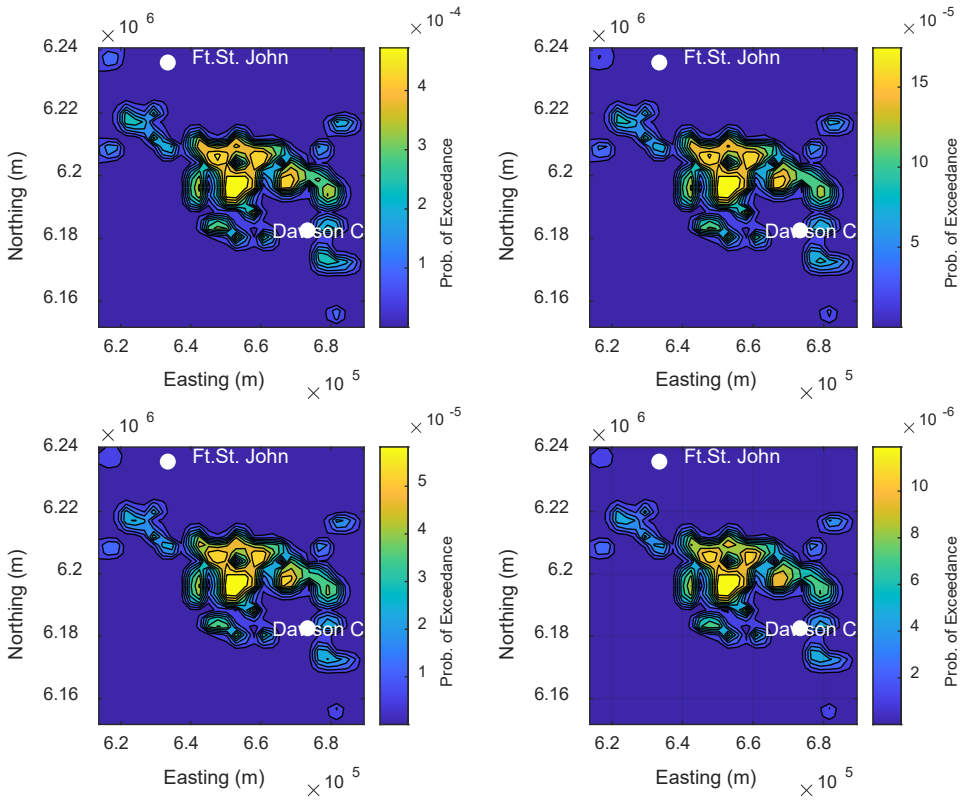

Figure 11 – $T = 0.4$ s, hazard $P[A > a]$, with $a = 0.05\ g$ (top left), $a = 0.1\ g$ (top right), $a = 0.2\ g$ (bottom left), and $a = 0.5\ g$ (bottom right).

9. Probability of Damage - Acceleration-Based

In this section, we present the calculated total probabilities of damage for the most resilient house (House 1) and the most vulnerable house (House 4). The calculated total probabilities of damage are presented for each limit state and for one year period in risk maps (Figures 13 and 14). Figure 12 and 13 reveal that the probability of damage of house 1 is larger than the one of house 4. This is somewhat surprising as the conditional probabilities of failure (Figure 6a and 6d) indicate that house 1 should be more resilient than house 4. This result can be explained considering the high-frequency ground motion hazard predicted by the GMM A-2015 (Atkinson, 2015). This point will be expanded later. Concerning the annual probability of failure, for each house model, the model confirms that the likelihood of experiencing damage decreases from F_{A1} to F_{A4}.

The spatial distribution of the probability of damage in the study area is affected by the ground motion hazard presented in the previous section of this paper, which is larger along an alignment that approximately follows the distance between Fort St. John and Dawson Creek. The largest probability of any damage is in an area of about 20 km^2 located 10 km north west of Dawson Creek and centered around the location having coordinates Easting 668,582 and Northing 6,196,200 (UTM zone 11). Since this area is affected by the largest seismic -induced risk, we summarize the calculated probabilities of damage in Table 5 for the injection period and in Table 6 for a period of 1 year. The tables also show the selected probability targets in red. From inspection of Tables 5 and 6, the following observations are made:

- For CLS (F_{A2}), the calculated probabilities of damage are lower than the targets; the predicted probabilities of damage are between two and four orders of magnitude lower than the targets for both the injection period and one year.
- For SLS (F_{A3}), the calculated probabilities of damage are lower than the targets; the predicted probabilities of damage are between one and three orders of magnitude lower than the targets for both the injection period and one year.
- For ULS (F_{A4}), the calculated probabilities of damage of Houses 2, 3, and 4 are lower than the proposed limits; the predicted probabilities of damage are between one and two orders of magnitude lower than the targets for both the injection period and one year.
- For ULS (F_{A4}), the calculated probability of damage for House 1 is three times larger than the target.
- The seismic resiliency of the house models considered in this study increases from House 1 to House 4. Despite House 1 model includes engineering solutions that make it the most resilient of the four for typical tectonic earthquakes, it could be the most vulnerable for induced earthquakes characterized by high-frequency ground motion hazard.

The last observation is not surprising considering that the fundamental period of House 1 is very close to the maximum predicted vibration period of the ground motion hazard. Figure 14 shows the acceleration spectra calculated at the location having coordinates Easting 668,582, Northing 6,196,200 (UTM zone 11), for M = 6 and for different hypocentral distances R. Figure 14 also

shows the location of the fundamental period of vibration of the four houses considered in this study. It can be observed the fundamental period of House 1 is the closest to the maximum of the ground motion spectra and therefore experiences the largest spectral acceleration. In addition, the spectral acceleration experienced from each house decreases rapidly moving from House 1 to House 4. As the hypocentral distance increases, the difference between the calculated accelerations at the different vibration periods become less important due to the flatter shape of the ground motion spectrum. Therefore, despite the largest resilience for tectonic earthquakes, usually characterized by longer periods than the induced earthquake, House 1 is the most vulnerable to high-frequency induced earthquakes and the calculated probability of ULS failure exceeds the limit. Also, when the hypocentral distance exceeds 10 km, the vulnerability of the houses is similar irrespective of their engineering properties.

Table 4 – Calculated probabilities of damage at Easting 668,582, Northing 6,196,200 (UTM zone 11) – Injection Period

		House 1	House 2	House 3	House 4
$P[A > C_{A2}]$	Acceleration - Based	5.7E-05	5.7E-06	6.9E-07	4.3E-07
	Limits	**1.0E-03**	**1.0E-03**	**1.0E-03**	**1.0E-03**
$[A > C_{A3}]$	Acceleration - Based	9.6E-05	8.4E-06	7.9E-07	5.2E-07
	Limits	**1.9E-04**	**1.9E-04**	**1.9E-04**	**1.9E-04**
$[A > C_{A4}]$	Acceleration - Based	1.3E-04	2.2E-05	1.8E-06	9.2E-07
	Limits	**3.8E-05**	**3.8E-05**	**3.8E-05**	**3.8E-05**

Table 5 – Calculated probabilities of damage at Easting 668,582, Northing 6,196,200 (UTM zone 11) – One year

		House 1	House 2	House 3	House 4
$[A > C_{A2}]_1$	Acceleration - Based	3.0E-03	3.0E-04	3.6E-05	2.2E-05
	Limits	**5.0E-02**	**5.0E-02**	**5.0E-02**	**5.0E-02**
$[A > C_{A3}]_1$	Acceleration - Based	5.0E-03	4.4E-04	4.1E-05	2.7E-05
	Limits	**1.0E-02**	**1.0E-02**	**1.0E-02**	**1.0E-02**
$[A > C_{A2}]_1$	Acceleration - Based	5.0E-03	4.4E-04	4.1E-05	2.7E-05
	Limits	**2.0E-03**	**2.0E-03**	**2.0E-03**	**2.0E-03**

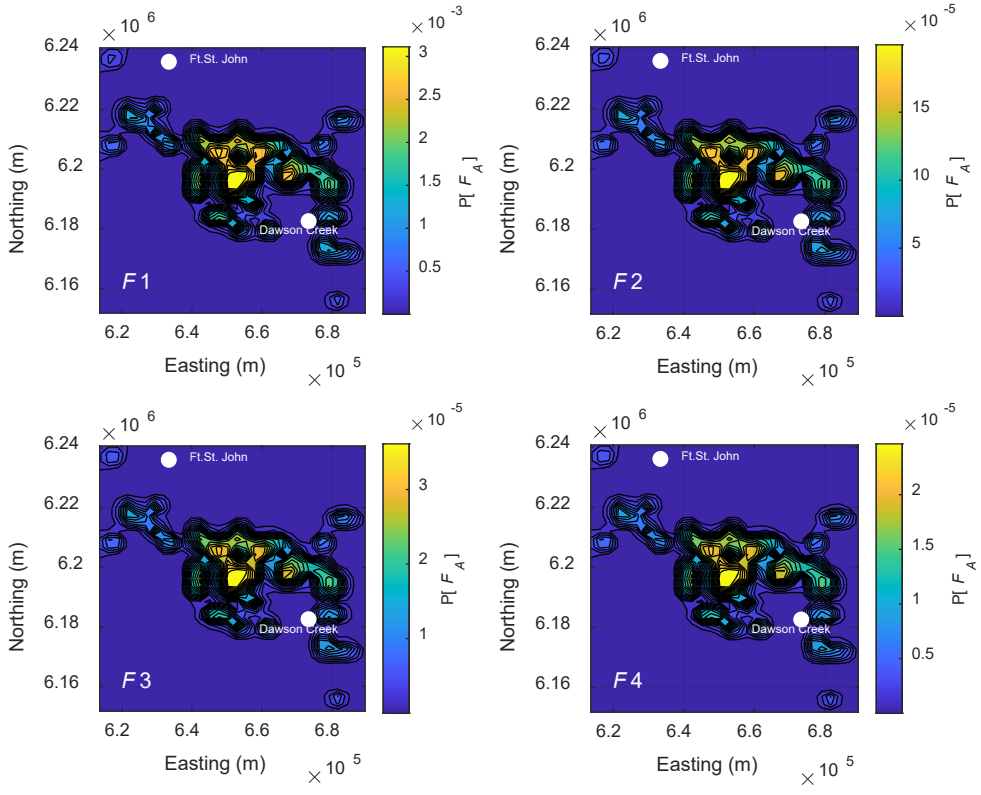

Figure 12 - P$[F_{Ai}]_1$ for house 1, 1 year

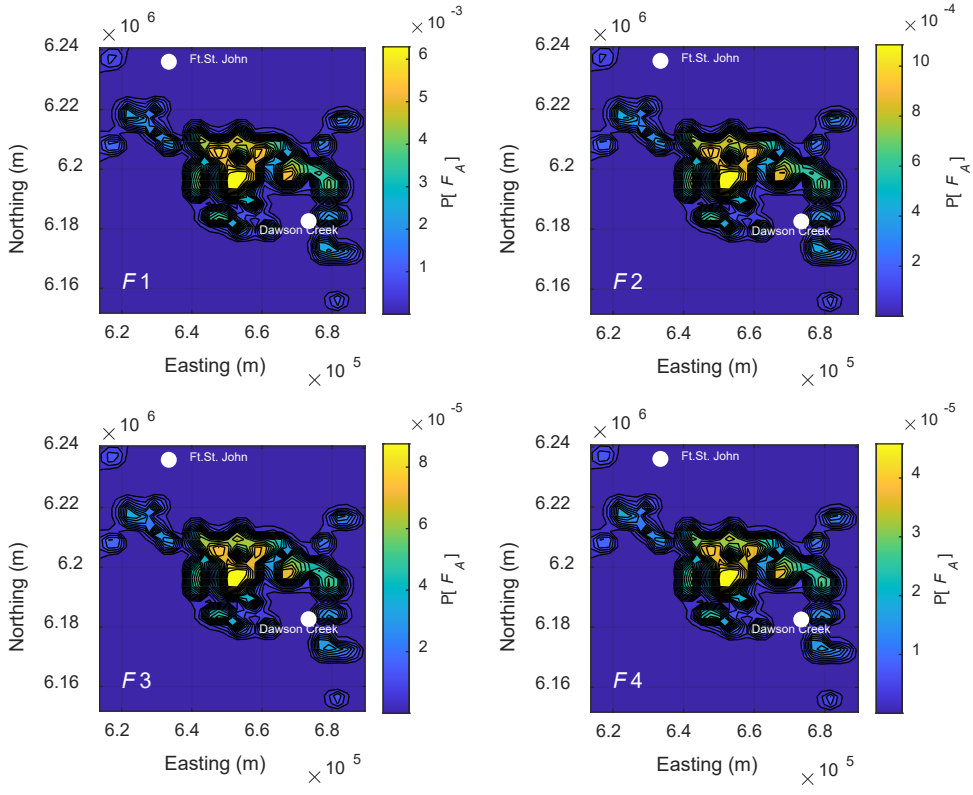

Figure 13 - $P[F_{Ai}]_1$ for house 4, 1 year

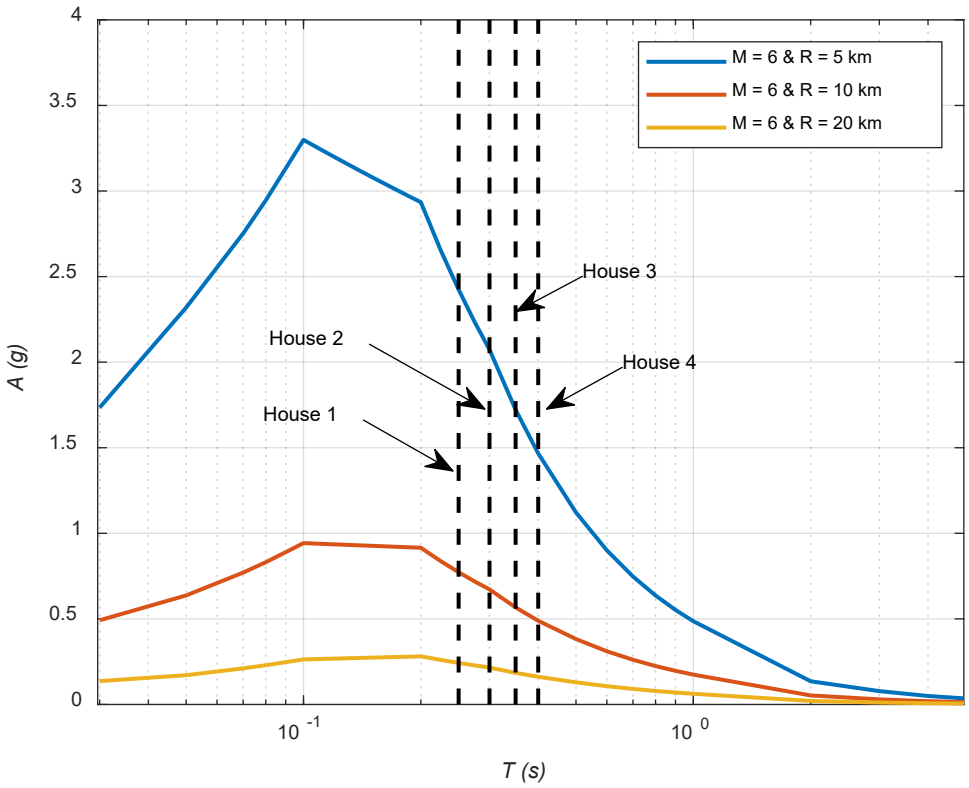

Figure 14 – Mean acceleration spectra at Easting 668,582, Northing 6,196,200 (UTM zone 11) for M = 6 and different hypocentral distances R

10.Probability of Velocity-Based Damage for CLS

The velocity-based probabilities of damage for CLS are presented in Figures 15 and 16 for the most resilient house (House 1) and the most vulnerable one (House 4). The velocity-based risk follows the same spatial distribution of the acceleration-based risk. The probability of damage is affected by the ground motion hazard presented in the previous section of this paper, which is larger along an alignment that approximately follows the distance between Fort St. John and Dawson Creek. Also for PPV, the largest probability of any damage is in the area centered around the location having coordinates Easting 668,582 and Northing 6,196,200 (UTM zone 11). For this location, the calculated probabilities of damage are summarized in Table 6 for the injection period and in Table 7 for a period of 1 year. The tables also show the probability targets in red.

From inspection of the figures and the tables, the following is observed:

- For CLS (F_{V2}), the calculated probabilities of damage are lower than the proposed targets; the predicted probabilities of damage are two orders of magnitude lower than the targets for both the injection period and one year.
- For CLS (F_{V2}), the calculated probabilities of damage are larger than the acceleration-based ones. Moving from House 1 to House 4, $P[F_{V2}]$ and $P[F_{V2}]_1$ are between 2 times and 2 order of magnitudes larger than the acceleration-based ones.
- The difference between the velocity-based , $P[F_{V2}]$ calculated for different materials and different house-models are small as the PPV targets are very similar and frequency-independent.

Table 6 – Calculated probabilities of damage at Easting 668,582, Northing 6,196,200 (UTM zone 11) – Injection Period

		House 1	House 2	House 3	House 4
$P[V > C_{V2}]$	Plaster Velocity - Based	9.6E-05	9.6E-05	9.6E-05	9.9E-05
	Drywall Velocity - Based	9.2E-05	9.4E-05	9.6E-05	9.9E-05
	Limits	**1.0E-03**	**1.0E-03**	**1.0E-03**	**1.0E-03**

Table 7 – Calculated probabilities of damage at Easting 668,582, Northing 6,196,200 (UTM zone 11) – One year

		House 1	House 2	House 3	House 4
$P[V > C_{V2}]_1$	Plaster Velocity - Based	5.0E-03	5.0E-03	5.0E-03	5.1E-03
	Drywall Velocity - Based	4.8E-03	4.9E-03	5.0E-03	5.1E-03
	Limits	**5.0E-02**	**5.0E-02**	**5.0E-02**	**5.0E-02**

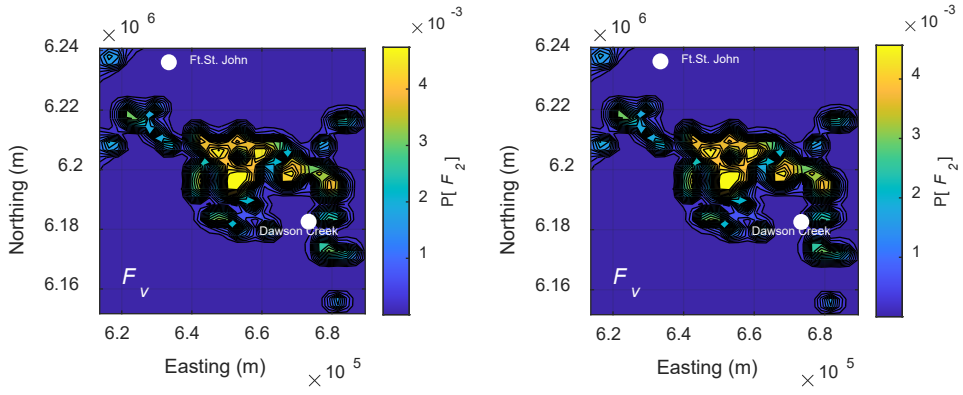

Figure 16 - $P[V > C_{V2}]_1$ for house 1, 1 year, plaster is the left figure, drywall is the right figure

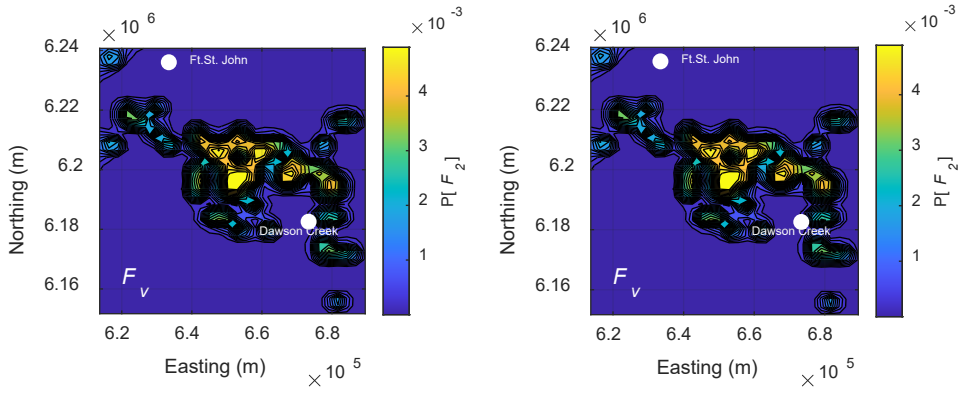

Figure 17 - $P[V > C_{V2}]_1$ for house 4, 1 year, plaster is the left figure, drywall is the right figure

11.Conclusions and Recommendations

In this study, we estimated the risk of damage for residential timber frames in the KSSMA for three limit states, the CLS, the SLS, and the ULS. For this purpose, we developed a short-term ground motion probabilistic hazard derived from the one recently published by Tang and Baker (2020) and successively modified by Esposito and Fenton (2022). The modifications of the original Tang and Baker (2020) model include the following:

- The hazard is defined in terms of probabilities of exceedance rather than rates of exceedance.
- We use a different form of the truncated Gutenberg-Richter distribution for the SMM, where the maximum magnitude m_{max} is estimated applying the extreme value distribution of the observed magnitudes.
- We include the variability of the distance between site and hypocenter and of the spectral acceleration produced by GMM A2015 (Atkinson, 2015) in the hazard model.

We consider two methodologies to assess the damage risk of the residential timber frames. First we derive the capacity for the different limit states considering both an acceleration-based conditional probability of failure derived from Goda (2019) and White and Ventura (2006), and a velocity-based conditional probability of failure based on USBM RI 8507 (USBM, 1983). The latter is a new methodology that applies a probabilistic interpretation of USBM RI 8507 (USBM, 1983). Finally, the risk of exceeding a limit state is calculated applying the total probability theorem which convolves the ground motion hazard and the timber frames conditional probabilities of failure. The result is a set of risk maps for the house models and different limit states to guide the responsible production activity in the area. The probabilities of damage are then compared to targets derived from international codes and standards. Canadian standards do not offer specific guidance on the acceptable probabilities of exceedance for the three limit states considered in this study. Four different timber frames were modelled, with House 1 being the most resilient to natural earthquakes and House 4 the most vulnerable.

From the results, the following conclusions can be drawn:

1. A strip running approximately along the distance between Dawson Creek and Fort. St. John is the area where the risk is the largest. This corresponds to the area where, between 2017 and 2018, most of the hydraulic fracturing activity took place (Figure 2). This implies that most of the well completions in the study area in the period between 2017 and 2018 were seismogenic.
2. Inside this strip, an area of about 20 km^2 located 10 km northwest of Dawson Creek and centered around Easting 668,582 and Northing 6,196,200 (UTM zone 11) is where the risk is the largest.
3. In this critical area, the acceleration-based model that we used in this study predicts probabilities of damage for any limit state and any location always smaller than the

proposed damage limits, except for the ULS of House 1. Its ULS probability of exceedance is 3 times larger than the assumed target.

4. The exceedance of the ULS for House 1 is caused by the GMM A2015 which predicts the highest ground motion intensity at a relatively small period of vibration. Since House 1 is a rigid frame having a low period of vibration similar to the GMM A2015 ground motion intensity period of vibration, the resulting probability of damage is high.
5. The velocity-based model that we used in this study predicts probabilities of cosmetic damage always smaller than the proposed limits.

In this study we have introduced a PPV-based conditional probability of failure for cosmetic damage. This allows the probabilistic assessment of cosmetic damage for a large area or portfolio of similar buildings. This methodology is novel, therefore it should be validated through a program including the characterization of the residential timber frames in the area and through vibration measurements. This would help creating a baseline for assessing cosmetic damage claims and guiding industry and regulator in managing the induced-seismicity risk in the area.

Acknowledgements

The financial support of BC OGRIS is greatly acknowledged.

12. References

Atkinson, G. M. (2015). Ground-motion prediction equation for small-to-moderate events at short hypocentral distances, with application to induced-seismicity hazards, Bull. Seismol. Soc. Am. 105, no. 2A, doi:10.1785/0120140142.

Atkinson, G. M., H. Ghofrani H., Assatourians, K., 2015. Impact of Induced Seismicity on the Evaluation of Seismic Hazard: Some Preliminary Considerations. Seismological Research Letters 86(3):1009-1021 DOI: 10.1785/0220140204

Baker, J. W., Bradley, B. A., and Stafford, P. J. (2021). Seismic Hazard and Risk Analysis. Cambridge University Press, Cambridge, England.

Deutsch, C.V. and Journel, A.G., (1997). GSLIB Geostatistical Software Library and User's Guide, Oxford University Press, New York, second edition. 369 pages.

Esposito, G., and Fenton, G.A., 2022. Vulnerability of Small Dams Subject to Induced Seismicity in Northeast British Columbia. Proceeding of GeoCalgary 2022.

Fenton, G.A., and Griffiths, D. V. 2008. Risk Assessment in Geotechnical Engineering. John Wiley and Sons, Hoboken, NJ.

Ghofrani, H., and G. M. Atkinson (2020). Activation Rate of Seismicity for Hydraulic Fracture Wells in the Western Canada Sedimentary Basin, Bull. Seismol. Soc. Am. XX, 1–20, doi: 10.1785/0120200002

Ghofrani, H., G. M. Atkinson, Schultz, R., (2019). Short-Term Hindcasts of Seismic Hazard in the Western Canada Sedimentary Basin Caused by Induced and Natural Earthquakes. Seismological Research Letters – doi: 10.1785/0220180285

Goda, K., (2019). Nationwide Earthquake Risk Model for Wood-Frame Houses in Canada. Front. Built Environ. 5:128. doi: 10.3389/fbuil.2019.00128

Marzocchi, W., Sandri, L., 2007. A technical note on the bias in the estimation of the b-value and its uncertainty through the Least Squares technique. Annals of geophysics 50(3) DOI: 10.4401/ag-4422.

Marzocchi, W., and L. Sandri, 2003. A review and new insights on the estimation of the b- value and its uncertainty, Annals of geophysics, 46(December).

NRC, 2020. National building code of Canada. National Research Council of Canada, Ottawa

Schultz, Ryan, Beroza, G. C., Ellsworth, W. L., and Baker, J. W. (2020). "Risk-informed recommendations for managing hydraulic fracturing induced seismicity via traffic light protocols." Bulletin of the Seismological Society of America, 110(5), 2411-2422.

Teng, G., and Baker, J. W. (2020). “Short-term probabilistic hazard assessment in regions of induced seismicity.” Bulletin of the Seismological Society of America, 110(5), 2441-2453.

Visser, R., H Kao, B Smith, C Goerzen, B Kontou, RMH Dokht, (2019), A comprehensive earthquake catalogue for the Fort St. John–Dawson Creek region, British Columbia, 2017–2018, Tech. rep., Open File 8718, Geological Survey of Canada.

White, T. W., and Ventura, C. E. (2006). Seismic Performance of Wood-frame Residential Construction in British Columbia-Technical Report. Earthquake Eng. Research Facility Report No. 06-03. Vancouver, BC: University of British Columbia.


DALHOUSIE
UNIVERSITY